EUROPEAN ORGANISATION FOR NUCLEAR RESEARCH

CERN-PPE/96-100
July 19, 1996

Σ^+, Σ^0 and Σ^- Hyperon Production in Hadronic Z^0 Decays

The OPAL Collaboration

Abstract

The production rates of the $J^P = \frac{1}{2}^+$ octet Σ baryons in hadronic Z^0 decays have been measured using the OPAL detector at LEP. The inclusive production rates per hadronic Z^0 decay of the three isospin states (including the respective antiparticle) have been separately measured for the first time:

$$\begin{aligned} n_{\Sigma^+} &= 0.099 \pm 0.008 \pm 0.013 \\ n_{\Sigma^0} &= 0.071 \pm 0.012 \pm 0.013 \\ n_{\Sigma^-} &= 0.083 \pm 0.006 \pm 0.009, \end{aligned}$$

where the first error is statistical and the second is systematic. Differential cross-sections are also presented for the Σ^+ and Σ^- and compared with JETSET and HERWIG predictions. Assuming full isospin symmetry, the average inclusive rate is:

$$\frac{1}{3}[n_{\Sigma^+ + \Sigma^0 + \Sigma^-}] = 0.084 \pm 0.005 \text{ (stat.)} \pm 0.008 \text{ (syst.)} .$$

(Submitted to Z. Phys.)

The OPAL Collaboration

G. Alexander[23], J. Allison[16], N. Altekamp[5], K. Ametewee[25], K.J. Anderson[9], S. Anderson[12], S. Arcelli[2], S. Asai[24], D. Axen[29], G. Azuelos[18,a], A.H. Ball[17], E. Barberio[8], R.J. Barlow[16], R. Bartoldus[3], J.R. Batley[5], J. Bechtluft[14], C. Beeston[16], T. Behnke[8], A.N. Bell[1], K.W. Bell[20], G. Bella[23], S. Bentvelsen[8], P. Berlich[10], S. Bethke[14], O. Biebel[14], V. Blobel[8], I.J. Bloodworth[1], J.E. Bloomer[1], M. Bobinski[10], P. Bock[11], H.M. Bosch[11], M. Boutemeur[34], B.T. Bouwens[12], S. Braibant[12], R.M. Brown[20], H.J. Burckhart[8], C. Burgard[8], R. Bürgin[10], P. Capiluppi[2], R.K. Carnegie[6], A.A. Carter[13], J.R. Carter[5], C.Y. Chang[17], C. Charlesworth[6], D.G. Charlton[1,b], D. Chrisman[4], S.L. Chu[4], P.E.L. Clarke[15], I. Cohen[23], J.E. Conboy[15], O.C. Cooke[16], M. Cuffiani[2], S. Dado[22], C. Dallapiccola[17], G.M. Dallavalle[2], S. De Jong[12], L.A. del Pozo[8], K. Desch[3], M.S. Dixit[7], E. do Couto e Silva[12], M. Doucet[18], E. Duchovni[26], G. Duckeck[34], I.P. Duerdoth[16], J.E.G. Edwards[16], P.G. Estabrooks[6], H.G. Evans[9], M. Evans[13], F. Fabbri[2], P. Fath[11], F. Fiedler[12], M. Fierro[2], H.M. Fischer[3], R. Folman[26], D.G. Fong[17], M. Foucher[17], A. Fürtjes[8], P. Gagnon[7], A. Gaidot[21], J.W. Gary[4], J. Gascon[18], S.M. Gascon-Shotkin[17], N.I. Geddes[20], C. Geich-Gimbel[3], F.X. Gentit[21], T. Geralis[20], G. Giacomelli[2], P. Giacomelli[4], R. Giacomelli[2], V. Gibson[5], W.R. Gibson[13], D.M. Gingrich[30,a], D. Glenzinski[9], J. Goldberg[22], M.J. Goodrick[5], W. Gorn[4], C. Grandi[2], E. Gross[26], M. Gruwé[8], C. Hajdu[32], G.G. Hanson[12], M. Hansroul[8], M. Hapke[13], C.K. Hargrove[7], P.A. Hart[9], C. Hartmann[3], M. Hauschild[8], C.M. Hawkes[5], R. Hawkings[8], R.J. Hemingway[6], G. Herten[10], R.D. Heuer[8], M.D. Hildreth[8], J.C. Hill[5], S.J. Hillier[1], T. Hilse[10], P.R. Hobson[25], R.J. Homer[1], A.K. Honma[28,a], D. Horváth[32,c], R. Howard[29], R.E. Hughes-Jones[16], D.E. Hutchcroft[5], P. Igo-Kemenes[11], D.C. Imrie[25], M.R. Ingram[16], K. Ishii[24], A. Jawahery[17], P.W. Jeffreys[20], H. Jeremie[18], M. Jimack[1], A. Joly[18], C.R. Jones[5], G. Jones[16], M. Jones[6], R.W.L. Jones[8], U. Jost[11], P. Jovanovic[1], T.R. Junk[8], D. Karlen[6], K. Kawagoe[24], T. Kawamoto[24], R.K. Keeler[28], R.G. Kellogg[17], B.W. Kennedy[20], B.J. King[8], J. Kirk[29], S. Kluth[8], T. Kobayashi[24], M. Kobel[10], D.S. Koetke[6], T.P. Kokott[3], S. Komamiya[24], R. Kowalewski[8], T. Kress[11], P. Krieger[6], J. von Krogh[11], P. Kyberd[13], G.D. Lafferty[16], H. Lafoux[21], R. Lahmann[17], W.P. Lai[19], D. Lanske[14], J. Lauber[15], S.R. Lautenschlager[31], J.G. Layter[4], D. Lazic[22], A.M. Lee[31], E. Lefebvre[18], D. Lellouch[26], J. Letts[2], L. Levinson[26], C. Lewis[15], S.L. Lloyd[13], F.K. Loebinger[16], G.D. Long[17], M.J. Losty[7], J. Ludwig[10], A. Luig[10], A. Malik[21], M. Mannelli[8], S. Marcellini[2], C. Markus[3], A.J. Martin[13], J.P. Martin[18], G. Martinez[17], T. Mashimo[24], W. Matthews[25], P. Mättig[3], W.J. McDonald[30], J. McKenna[29], E.A. Mckigney[15], T.J. McMahon[1], A.I. McNab[13], R.A. McPherson[8], F. Meijers[8], S. Menke[3], F.S. Merritt[9], H. Mes[7], J. Meyer[27], A. Michelini[2], G. Mikenberg[26], D.J. Miller[15], R. Mir[26], W. Mohr[10], A. Montanari[2], T. Mori[24], M. Morii[24], U. Müller[3], K. Nagai[26], I. Nakamura[24], H.A. Neal[8], B. Nellen[3], B. Nijjhar[16], R. Nisius[8], S.W. O'Neale[1], F.G. Oakham[7], F. Odorici[2], H.O. Ogren[12], T. Omori[24], M.J. Oreglia[9], S. Orito[24], J. Pálinkás[33,d], G. Pásztor[32], J.R. Pater[16], G.N. Patrick[20], J. Patt[10], M.J. Pearce[1], S. Petzold[27], P. Pfeifenschneider[14], J.E. Pilcher[9], J. Pinfold[30], D.E. Plane[8], P. Poffenberger[28], B. Poli[2], A. Posthaus[3], H. Przysiezniak[30], D.L. Rees[1], D. Rigby[1], S.A. Robins[13], N. Rodning[30], J.M. Roney[28], A. Rooke[15], E. Ros[8], A.M. Rossi[2], M. Rosvick[28], P. Routenburg[30], Y. Rozen[22], K. Runge[10], O. Runolfsson[8], U. Ruppel[14], D.R. Rust[12], R. Rylko[25], K. Sachs[10], E.K.G. Sarkisyan[23], M. Sasaki[24], C. Sbarra[2], A.D. Schaile[34], O. Schaile[34], F. Scharf[3], P. Scharff-Hansen[8], P. Schenk[4], B. Schmitt[8], S. Schmitt[11], M. Schröder[8], H.C. Schultz-Coulon[10], M. Schulz[8], M. Schumacher[3], P. Schütz[3], W.G. Scott[20], T.G. Shears[16], B.C. Shen[4], C.H. Shepherd-Themistocleous[27], P. Sherwood[15], G.P. Siroli[2], A. Sittler[27], A. Skillman[15], A. Skuja[17], A.M. Smith[8], T.J. Smith[28], G.A. Snow[17], R. Sobie[28], S. Söldner-Rembold[10], R.W. Springer[30], M. Sproston[20], A. Stahl[3],

M. Starks[12], M. Steiert[11], K. Stephens[16], J. Steuerer[27], B. Stockhausen[3], D. Strom[19], F. Strumia[8], P. Szymanski[20], R. Tafirout[18], S.D. Talbot[1], S. Tanaka[24], P. Taras[18], S. Tarem[22], M. Tecchio[8], M. Thiergen[10], M.A. Thomson[8], E. von Törne[3], S. Towers[6], T. Tsukamoto[24], E. Tsur[23], A.S. Turcot[9], M.F. Turner-Watson[8], P. Utzat[11], R. Van Kooten[12], G. Vasseur[21], M. Verzocchi[10], P. Vikas[18], M. Vincter[28], E.H. Vokurka[16], F. Wäckerle[10], A. Wagner[27], C.P. Ward[5], D.R. Ward[5], J.J. Ward[15], P.M. Watkins[1], A.T. Watson[1], N.K. Watson[7], P. Weber[6], P.S. Wells[8], N. Wermes[3], J.S. White[28], B. Wilkens[10], G.W. Wilson[27], J.A. Wilson[1], G. Wolf[26], S. Wotton[5], T.R. Wyatt[16], S. Yamashita[24], G. Yekutieli[26], V. Zacek[18],

[1]School of Physics and Space Research, University of Birmingham, Birmingham B15 2TT, UK
[2]Dipartimento di Fisica dell' Università di Bologna and INFN, I-40126 Bologna, Italy
[3]Physikalisches Institut, Universität Bonn, D-53115 Bonn, Germany
[4]Department of Physics, University of California, Riverside CA 92521, USA
[5]Cavendish Laboratory, Cambridge CB3 0HE, UK
[6] Ottawa-Carleton Institute for Physics, Department of Physics, Carleton University, Ottawa, Ontario K1S 5B6, Canada
[7]Centre for Research in Particle Physics, Carleton University, Ottawa, Ontario K1S 5B6, Canada
[8]CERN, European Organisation for Particle Physics, CH-1211 Geneva 23, Switzerland
[9]Enrico Fermi Institute and Department of Physics, University of Chicago, Chicago IL 60637, USA
[10]Fakultät für Physik, Albert Ludwigs Universität, D-79104 Freiburg, Germany
[11]Physikalisches Institut, Universität Heidelberg, D-69120 Heidelberg, Germany
[12]Indiana University, Department of Physics, Swain Hall West 117, Bloomington IN 47405, USA
[13]Queen Mary and Westfield College, University of London, London E1 4NS, UK
[14]Technische Hochschule Aachen, III Physikalisches Institut, Sommerfeldstrasse 26-28, D-52056 Aachen, Germany
[15]University College London, London WC1E 6BT, UK
[16]Department of Physics, Schuster Laboratory, The University, Manchester M13 9PL, UK
[17]Department of Physics, University of Maryland, College Park, MD 20742, USA
[18]Laboratoire de Physique Nucléaire, Université de Montréal, Montréal, Quebec H3C 3J7, Canada
[19]University of Oregon, Department of Physics, Eugene OR 97403, USA
[20]Rutherford Appleton Laboratory, Chilton, Didcot, Oxfordshire OX11 0QX, UK
[21]CEA, DAPNIA/SPP, CE-Saclay, F-91191 Gif-sur-Yvette, France
[22]Department of Physics, Technion-Israel Institute of Technology, Haifa 32000, Israel
[23]Department of Physics and Astronomy, Tel Aviv University, Tel Aviv 69978, Israel
[24]International Centre for Elementary Particle Physics and Department of Physics, University of Tokyo, Tokyo 113, and Kobe University, Kobe 657, Japan
[25]Brunel University, Uxbridge, Middlesex UB8 3PH, UK
[26]Particle Physics Department, Weizmann Institute of Science, Rehovot 76100, Israel
[27]Universität Hamburg/DESY, II Institut für Experimental Physik, Notkestrasse 85, D-22607 Hamburg, Germany
[28]University of Victoria, Department of Physics, P O Box 3055, Victoria BC V8W 3P6, Canada
[29]University of British Columbia, Department of Physics, Vancouver BC V6T 1Z1, Canada

[30]University of Alberta, Department of Physics, Edmonton AB T6G 2J1, Canada
[31]Duke University, Dept of Physics, Durham, NC 27708-0305, USA
[32]Research Institute for Particle and Nuclear Physics, H-1525 Budapest, P O Box 49, Hungary
[33]Institute of Nuclear Research, H-4001 Debrecen, P O Box 51, Hungary
[34]Ludwigs-Maximilians-Universität München, Sektion Physik, Am Coulombwall 1, D-85748 Garching, Germany

[a] and at TRIUMF, Vancouver, Canada V6T 2A3
[b] and Royal Society University Research Fellow
[c] and Institute of Nuclear Research, Debrecen, Hungary
[d] and Department of Experimental Physics, Lajos Kossuth University, Debrecen, Hungary

1 Introduction

Measurements of the various particle production rates and their differential cross-sections are essential for the construction of the phenomenological models that describe the hadronisation of quarks and gluons in jets[1, 2, 3]. To explain the baryon production rates, the models must reproduce the probability of producing a bound state of three quarks (or antiquarks) of varying flavour and spin content. Measurements performed using low energy e^+e^- annihilations and using LEP data[4, 6, 7] show that the production of baryons with high spin and/or strangeness content is suppressed. However, the measurements are insufficient to constrain the models fully, and it is necessary to measure as many of the octet and decuplet baryon rates as possible, as well as their energy distribution.

This paper presents a measurement of the three isospin states of the $J^P = \frac{1}{2}^+$ octet Σ baryon[1] in e^+e^- annihilation at centre-of-mass energies near the Z^0 peak, performed using the OPAL detector at LEP. For all three states (Σ^+, Σ^0 and Σ^-) the production rates have been measured as well as, for the charged states, the differential cross-sections. These results are compared to other strange baryon rates and to different model expectations.

Contrary to the naive expectation of isospin symmetry, the production rates of Σ^+, Σ^0 and Σ^- in Z^0 decay may not be the same. For example, in current models[1], the decay of a charm baryon produces the isospin $I_3 = +1$ state, Σ^+ (uus), more often than the $I_3 = -1$ state, Σ^- (dds), because the weak decay of a charm quark, $c \to s + W^+ \to s + u + \overline{d}$, yields quarks in a $I_3 = +1$ state. It is therefore of interest to measure the three isospin states separately.

The three Σ states all have different lifetimes and decay sequences and, consequently, different methods are used to reconstruct them. The Σ^0 decays electromagnetically 100 % of the time to $\Lambda\gamma$. It is reconstructed by combining Λ baryons reconstructed at secondary vertices with converted photons, both of which must be consistent with coming from the primary event vertex. The Σ^+ baryon, with $c\tau = 2.4$ cm, decays 51.6 % of the time to $p\pi^0$, and 48.3 % of the time to $n\pi^+$. Because of its non-zero lifetime, it is reconstructed by combining π^0 candidates with proton tracks which are not consistent with coming from the primary event vertex. Finally, the Σ^- baryon, with $c\tau = 4.4$ cm, decays almost 100 % of the time to $n\pi^-$. Because of its longer lifetime, it is often possible to reconstruct the primary Σ^- track, and its subsequent decay is sought by looking for its intersection with a secondary π^- track. The systematic errors of the three measurements are thus largely uncorrelated, reducing the error on the combined Σ^+, Σ^0 and Σ^- rate. As far as the measured rates are compatible with isospin symmetry, further gains in precision can be obtained by performing a weighted average.

2 The OPAL Detector

The OPAL detector and its performance have been described in detail elsewhere [8], so only items of importance for this analysis are mentioned. The central tracking system consists of three drift chambers which surround a silicon microvertex detector, all of which lie within

[1] Except where explicitly otherwise stated, charge conjugation is implied throughout this paper. Thus $\Sigma^+=(\Sigma^+ + \overline{\Sigma}^-)$, $\Sigma^0=(\Sigma^0 + \overline{\Sigma}^0)$ and $\Sigma^-=(\Sigma^- + \overline{\Sigma}^+)$.

an axial magnetic field of 0.435 T. On the outside lies a system of z-chambers, thin drift chambers, with a resolution of about 300 μm in the z coordinate[2], which serve to improve the determination of θ. Inside this is a large jet chamber, of outer radius 185 cm, which provides up to 159 digitisations per track with an xy resolution of around 130 μm. In addition, charged particles can be identified by their specific ionisation energy loss ($\mathrm{d}E/\mathrm{d}x$) in the jet chamber [10]. A precision vertex drift chamber of outer radius 24 cm provides space points with a resolution of about 50 μm in the xy plane and also has stereo wires, improving the z-resolution to approximately 1 mm. The resolution of the xy component of the track momentum (p_t) of the tracking chambers is $\sigma_{p_t}/p_t \sim \sqrt{(0.02)^2 + (0.0015 p_t)^2}$, where p_t is in GeV/c.

The high precision silicon microvertex detector [9] was installed in 1991. It has two layers, at about 6.1 and 7.5 cm from the beam axis, with an intrinsic resolution of 5 μm in the xy plane. In 1993, it was upgraded to supply additional tracking information in the z-coordinate, with an intrinsic z resolution of 13 μm.

Outside the tracking detectors and the magnet coil lies the barrel electromagnetic calorimeter, consisting of a cylindrical array of 9,440 lead glass blocks of 24.6 radiation lengths (X_0) thickness, and covering the polar angle range $|\cos\theta| < 0.82$ at a radius of 2.45 m. The overall energy resolution is improved by correcting for the energy lost in showers initiated in the material in front of the calorimeter. These showers are detected by thin gas detectors (presamplers) situated just in front of the lead glass blocks. Time-of-flight scintillators, situated between the presampler and the magnet coil in the polar angle range $|\cos\theta| < 0.72$, are also used to detect these showers.

3 Data Selection

In the years from 1990 to 1994, OPAL collected approximately 3.5 million hadronic events at centre-of-mass energies close to the Z^0 peak. Hadronic events are selected using standard cuts as described in refs. [11]. The three Σ analyses impose different additional requirements on the status of the relevant detector sub-systems. The most significant of these is the requirement of silicon microvertex information for the Σ^+ analysis, which reduces the number of events to 2.8 million.

The efficiencies for the three analyses are evaluated using 7 million simulated hadronic events generated by the Monte Carlo program JETSET [1] tuned so that it reproduces many of the global features of multihadronic events as observed at LEP [12]. The events are passed through a full simulation of the OPAL detector [13], including the event reconstruction software, and subjected to the same selections as the real data. It was checked that the Monte Carlo is able to reproduce adequately all the variables of importance for the following analyses. Where small deviations were found, their impacts on the systematic error are taken into account.

In all three analyses, cuts are made on the impact parameters of tracks with respect to the primary event vertex. This vertex is determined for every event using all charged tracks

[2]The OPAL coordinate system is defined so that z is the coordinate parallel to the e^- beam, r is the coordinate normal to this axis, θ is the polar angle with respect to z and ϕ is the azimuthal angle about the z-axis.

consistent with a common origin, using the average beam position as a constraint. The impact parameter of a charged track, d_0, is defined as the distance of closest approach to this primary vertex in the xy plane. The z_0 of a charged track is defined as its z coordinate at the point of closest approach in xy.

4 $\Sigma^+ \to p\pi^0$ Analysis

The Σ^+ baryon is identified via its decay channel $p\pi^0$. For example, a 5 GeV Σ^+ will decay typically 7.5 cm away from the beam axis, producing a proton track with a median impact parameter relative to the event vertex of $\sim$0.15 cm. Therefore, the proton candidates are chosen as tracks in the central detector having a significantly non-zero value of d_0 and also a measured dE/dx consistent with that of a proton. The π^0 mesons are reconstructed by combining pairs of photon candidates which are detected either as a localised energy deposit in the electromagnetic calorimeter, or as two tracks from a conversion within the volume of the central drift chambers. Proton and π^0 candidates are combined to form the Σ^+ baryon candidates.

4.1 Proton Selection

The proton candidates are selected by searching for tracks whose impact parameter, d_0, is more than 5 standard deviations away from zero. In addition, to reduce the contribution of tracks coming from hadronic interactions within the detector, both the d_0 and the z_0 of selected tracks must be less than 2 cm.

The purity of the proton candidate sample is further increased by imposing the following requirements on the dE/dx of the tracks. A track is accepted as a proton candidate if it has more than 40 dE/dx samples, and if the probability that its measured energy loss is consistent with the proton hypothesis is greater than 5 %. The large background from charged pions is reduced by requiring that the probability of the pion hypothesis be less than 5 %. Background from charged kaons mostly affects tracks with small impact parameters, since the lifetime of most kaon sources is short relative to that of the Σ^+. This background is reduced by requiring the measured dE/dx to be more consistent with the proton hypothesis than the kaon hypothesis when the d_0 of the track is less than 0.1 cm.

At this stage, a significant source of background in the sample comes from genuine protons produced in Λ decays. To reduce this background, the proton track is rejected if, in combination with any oppositely charged track in the event (assumed to be a pion), it has a mass within 8 MeV/c^2 of the nominal Λ mass [14]. In addition, the track is rejected if it is tagged by the Λ finder (method 2) described in ref. [5].

The determination of the decay vertex of the Σ^+ relies heavily on the precise measurement of the proton trajectory. Therefore, it is required that there be a measurement of the z coordinate both at large radius from the z-chambers, and also near the vertex from either the stereo wires of the vertex chamber or from the silicon microvertex detector.

According to the Monte Carlo simulation, these cuts select 22 % of all protons from Σ^+ decays.

4.2 Photon and π^0 Selection

Photons used to reconstruct the π^0 mesons are reconstructed as energy deposits in the electromagnetic calorimeter. Alternatively, they may also be detected as two tracks from conversions in the tracking chambers. Photons reconstructed as conversions represent only 7.8 % of the total number of photon candidates. Their identification will be discussed in detail in section 5.2.

The location and deposited energy of showers in the electromagnetic calorimeter are obtained from a fit to the expected lateral distribution of energy in the lead glass calorimeter. The lateral spread of each shower is described by a sum of two exponentials whose parameters have been optimised using Monte Carlo. Photons below 0.5 GeV deposit most of their energy in a single block, but the fitting procedure allows a proper treatment of overlapping showers and is very efficient at finding photon candidates in high-multiplicity events. Since low-energy photons may lose a significant amount of energy by initiating a shower before reaching the calorimeter, the energy of the showers is corrected using the signal amplitude observed in the presampler situated in front of the calorimeter.

A shower is kept if it has at least 0.1 GeV in deposited energy, E_d, and a corrected energy (using the presampler), E_c, of at least 0.15 GeV. The momentum direction of the photon is evaluated assuming that it originates from the primary vertex. This is not strictly true for photons from a $\Sigma^+ \to p\pi^0$ decay, but is a sufficiently good approximation, given that the distance between the decay vertex and the electromagnetic calorimeter is large compared with the average Σ^+ decay length, and that the position resolution on the shower (a few cm) is on the same scale as the average Σ^+ decay length.

The π^0 candidates are obtained by combining in turn all pairs of photon candidates. The selection of the π^0 candidates makes use of an estimator, v, based on such quantities as the invariant mass and the opening angle of the pair, the number of neighbouring photons, the energy of the two photons, the energy deposited in their immediate vicinity, the distance to the closest charged particle track, the shower shape and the quality of the shower fit. The estimator is tuned on a sample of π^0 candidates from 50,000 simulated hadronic Z^0 decays. From that same simulation the probability that a pair is a genuine π^0 is evaluated as a function of the estimator value. Denoting as P_{ij} the probability that the pair involving the photons i and j is a genuine π^0, the following quantity is derived:

$$\tilde{P}_{ij} = P_{ij} \prod_{k \neq i,j} (1 - P_{ik}) \prod_{l \neq i,j} (1 - P_{jl}) \,. \qquad (1)$$

The quantity $\tilde{P}_{ij}$ is thus related to the probability that the pair (i,j) is a π^0 and that none of the other pairs in the event involving i or j is a π^0. The distribution of $\tilde{P}_{ij}$ for data and Monte Carlo samples is shown in figure 1a. The distribution is well reproduced by the Monte Carlo. Pairs with $\tilde{P}_{ij} > 0.1$ are retained, resulting in an efficiency of 8.6 % and a purity of 44 %. To illustrate further the reliability of the estimator, its invariant mass dependence is removed and the invariant mass of the pairs with $\tilde{P}_{ij} > 0.1$ is shown in figure 1b. Again, the data are well reproduced by the Monte Carlo.

Once a π^0 candidate is selected, the resolution on its energy is improved by constraining its mass to the nominal value [14] using a kinematic fit.

4.3 Σ^+ Reconstruction

Σ^+ candidates are obtained by combining the proton and π^0 candidates.

A good estimate of the Σ^+ momentum is made by combining the momenta of the π^0 with that of the proton defined at its point of closest approach to the primary vertex. It is then assumed that the Σ^+ originates at the primary vertex, which is reasonable since all particles which decay into Σ^+ have short lifetimes. Then, neglecting the curvature of the proton track, the decay length of the Σ^+ in the xy plane is $l_{xy} = d_0/\sin\psi$, where ψ is the angle in the xy plane between the proton and the Σ^+ momenta. The distribution of this variable is shown in fig. 2a for data and Monte Carlo events. Candidates with negative decay length are rejected.

The component of the Σ^+ flight distance in the z direction is estimated in two ways. In the first, this distance is obtained by projecting l_{xy} onto the flight direction of the Σ^+ defined by its momentum. In the second, it is obtained by projecting l_{xy} onto the proton track. The difference between the two z values, Δz, should be small for real Σ^+ candidates. Because of experimental resolution, $|\Delta z|$ is required to be less than 0.7 cm if the track has a z measurement from the vertex chamber stereo wires, and less than 0.3 cm if it has z information from the silicon microvertex detector. The distribution of this variable is shown in fig. 2b.

The proper time of the Σ^+ decay, t', can be evaluated from the measured decay length in 3 dimensions and the measured momentum. The decay probability, $\exp(-t'/\tau)$, where τ is the known lifetime of the Σ^+[14], is expected to be uniformly distributed between 0 and 1 in an unbiased Σ^+ sample. The pronounced increase toward 1.0 in fig. 2c is due to the background of tracks with very small impact parameters. Low-momentum particles with large impact parameters, such as protons generated in nuclear reactions within the detector material, have decay probabilities very close to zero. A cut of $0.01 < \exp(-t'/\tau) < 0.80$ is thus imposed.

The distribution of the difference between the radius of the first measured point on the proton track and the value of l_{xy} is shown in fig. 2d). This difference tends to be large and positive for the background arising from tracks originating from the primary vertex. For decays occuring well within the volume of the tracking detectors, the two values coincide to within a few centimeters. A candidate is rejected if the difference is larger than 3 cm. However, if the decay length is small, that difference may be as large as the radius of the innermost detector, the silicon microvertex. Therefore, if the first measured point is provided by this detector, this cut is relaxed to 5 cm.

4.4 Fit to the Signal

Figure 3 shows the invariant mass distribution of the proton-π^0 combinations, after all cuts. There is a clear peak at the Σ^+ mass (1189.4 MeV/c^2 [14]). The mass spectrum is fitted to a signal Gaussian plus a background parametrised as an exponential convoluted with a Gaussian.

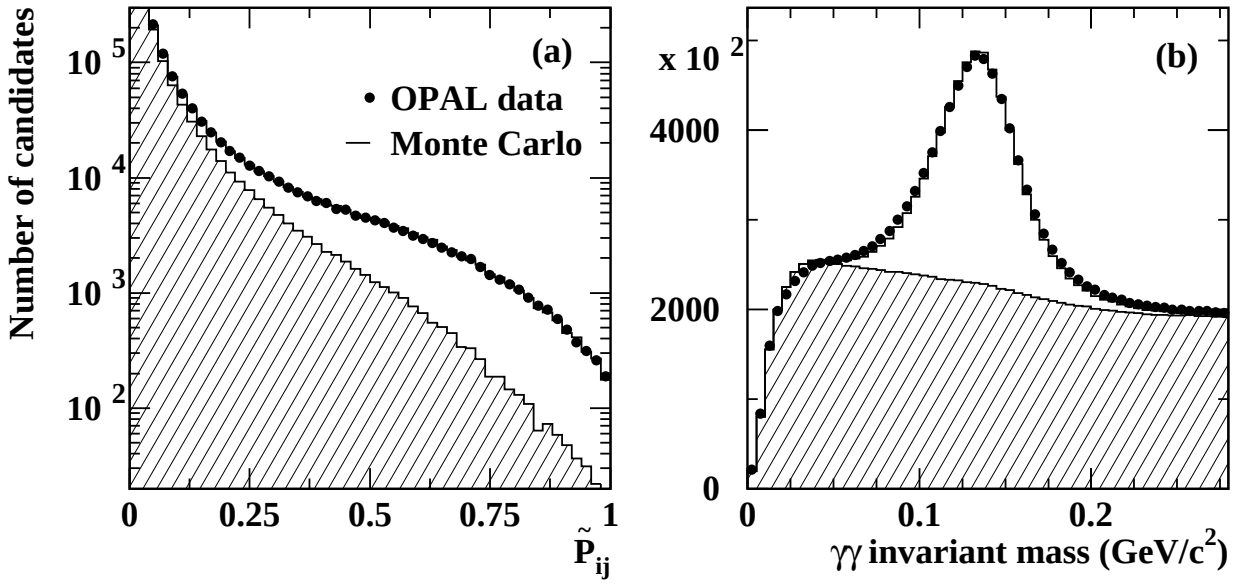

Figure 1: In these plots, the points represent OPAL data, the open histogram the Monte Carlo simulation normalised to the same number of events and the hatched histogram the expected background contribution. (a) Distribution of the variable $\tilde{P}_{ij}$ used for the selection of π^0 candidates (see text). (b) Invariant mass of pairs of photons obtained in a sample of 40,000 Z^0 decays, using the same cuts as used in the Σ^+ analysis, once the invariant mass dependence of the variable $\tilde{P}_{ij}$ is removed.

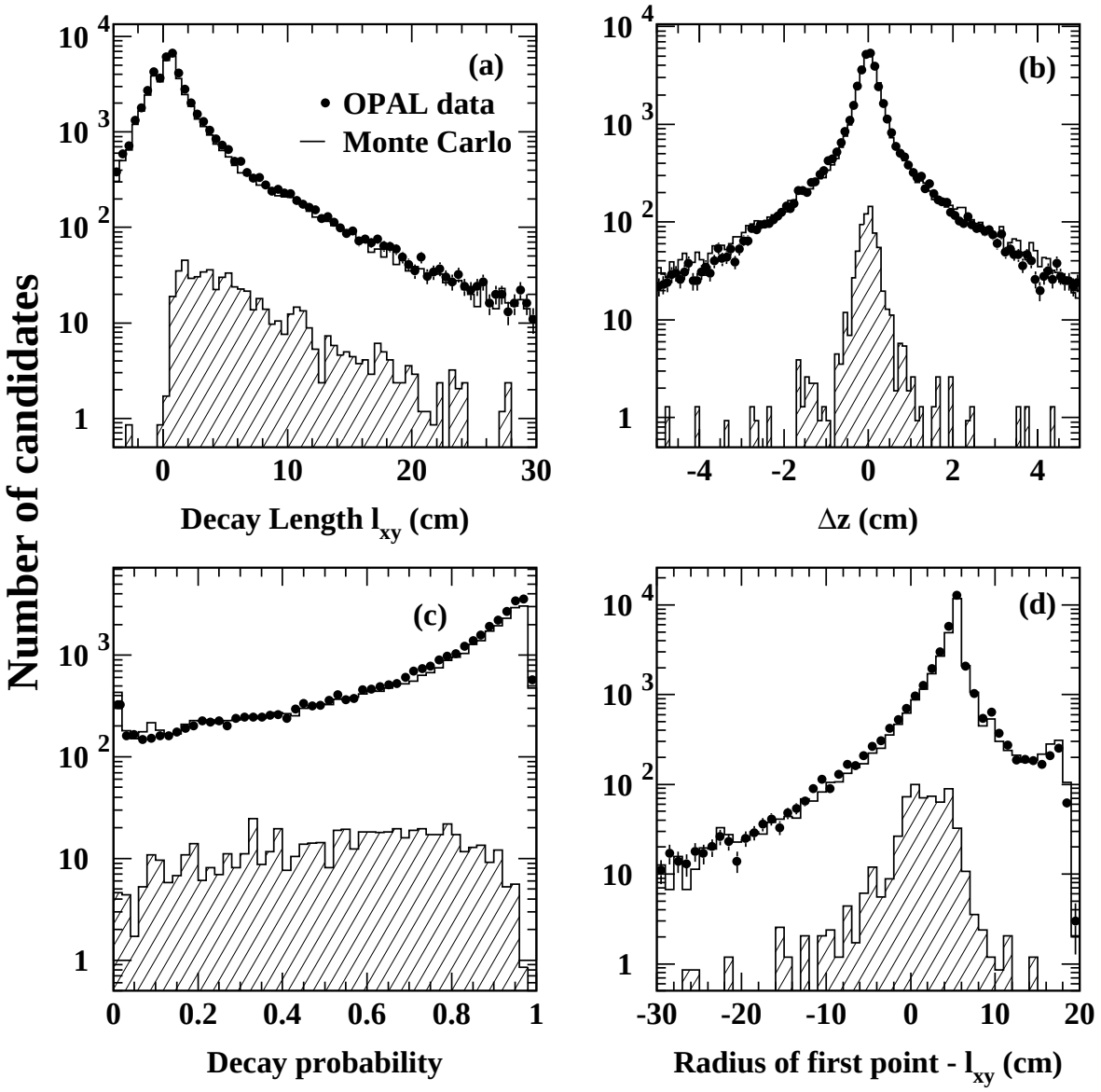

Figure 2: Distribution of some of the quantities used in the reconstruction of the $\Sigma^+ \to p\pi^0$ decay. In all plots, the points represent OPAL data, the open histogram the Monte Carlo simulation, and the hatched histogram represents the expected contribution from $\Sigma^+ \to p\pi^0$ decays. (a) Distribution of the reconstructed decay length l_{xy}. (b) Distribution of the quantity Δz (see text). (c) Distribution of the decay probability $\exp(-t'/\tau)$. (d) Difference between the decay length l_{xy} and the radius of the first measurement along the track.

The fitted signal Gaussian has a mean of 1187.4 $\pm$ 1.2 MeV/c^2, a width of 15.1 $\pm$ 1.4 MeV/c^2, and contains 621 $\pm$ 56 events. The width is consistent with that observed in the Monte Carlo sample (14.1 $\pm$ 0.4 MeV/c^2).

The differential cross-section, as a function of the scaled energy, $x_E = E_\Sigma / E_{\rm beam}$, is obtained from a fit to the data in 7 bins of x_E ranging from 0.04 to 0.4. In these fits, the mass is fixed to the fit value of 1187.4 MeV/c^2, and the width of the signal is set to the Monte Carlo prediction.

The energy-dependent efficiencies, listed in table 1, are obtained from the Monte Carlo sample. The efficiency-corrected rates of Σ^+ per hadronic Z^0 decay are listed in bins of x_E in table 1, and are shown in fig. 7.

x_E bin	Number of signal events	Efficiency (%)	Differential Cross-Section $\frac{1}{\sigma_{had}}\frac{d\sigma}{dx_E}$ ($\pm$ stat. $\pm$ syst. errors)
0.040 - 0.050	34.4 $\pm$ 8.7	0.147 $\pm$ 0.026	0.85 $\pm$ 0.22 $\pm$ 0.16
0.050 - 0.075	67.7 $\pm$ 12.3	0.111 $\pm$ 0.019	0.89 $\pm$ 0.16 $\pm$ 0.16
0.075 - 0.100	101.5 $\pm$ 18.5	0.382 $\pm$ 0.067	0.388 $\pm$ 0.071 $\pm$ 0.073
0.100 - 0.150	163.0 $\pm$ 24.9	0.458 $\pm$ 0.083	0.260 $\pm$ 0.040 $\pm$ 0.047
0.150 - 0.200	117.4 $\pm$ 17.2	0.420 $\pm$ 0.052	0.204 $\pm$ 0.030 $\pm$ 0.027
0.200 - 0.300	61.7 $\pm$ 16.1	0.246 $\pm$ 0.035	0.091 $\pm$ 0.024 $\pm$ 0.013
0.300 - 0.400	16.0 $\pm$ 7.2	0.121 $\pm$ 0.055	0.048 $\pm$ 0.022 $\pm$ 0.015

Table 1: Σ^+ detection efficiency (in per cent) and differential cross-section $\frac{1}{\sigma_{had}}\frac{d\sigma}{dx_E}$ in bins of x_E. The x_E range from 0.04 to 0.40 was chosen since only in this range were significant measurements of the number of events possible.

4.5 Consistency Checks and Systematic Errors

In this section we discuss the tests of consistency and the systematic errors on the measurements.

The rates obtained for the Σ^+ and $\overline{\Sigma^-}$ are equal within their statistical errors (283$\pm$40 and 304$\pm$33, respectively). The fraction of the total signal for which at least one of the photon candidates is a photon conversion is the same within errors in the data and in the Monte Carlo (14$\pm$3 % and 11$\pm$1 %, respectively). With the Monte Carlo sample, it was verified that no Σ^+ arising from hadronic interactions with the detector material survived the selection cuts. This rejection is mostly due to the smaller efficiency for low-energy Σ^+ and the primary vertex constraint used in the reconstruction.

The systematic errors are summarised in table 2. They are assumed to be fully correlated from one x_E bin to another, except for the error associated with the finite size of the Monte Carlo sample used to evaluate the efficiency which results in a 4.5% uncertainty on the integrated cross-section. The uncertainty on the branching ratio BR($\Sigma^+ \to p\pi^0$) is very small (0.6%).

The uncertainty on the fit procedure was evaluated for each x_E bin separately by systematicaly varying the width of the signal and the parametrisation of the background. The fits

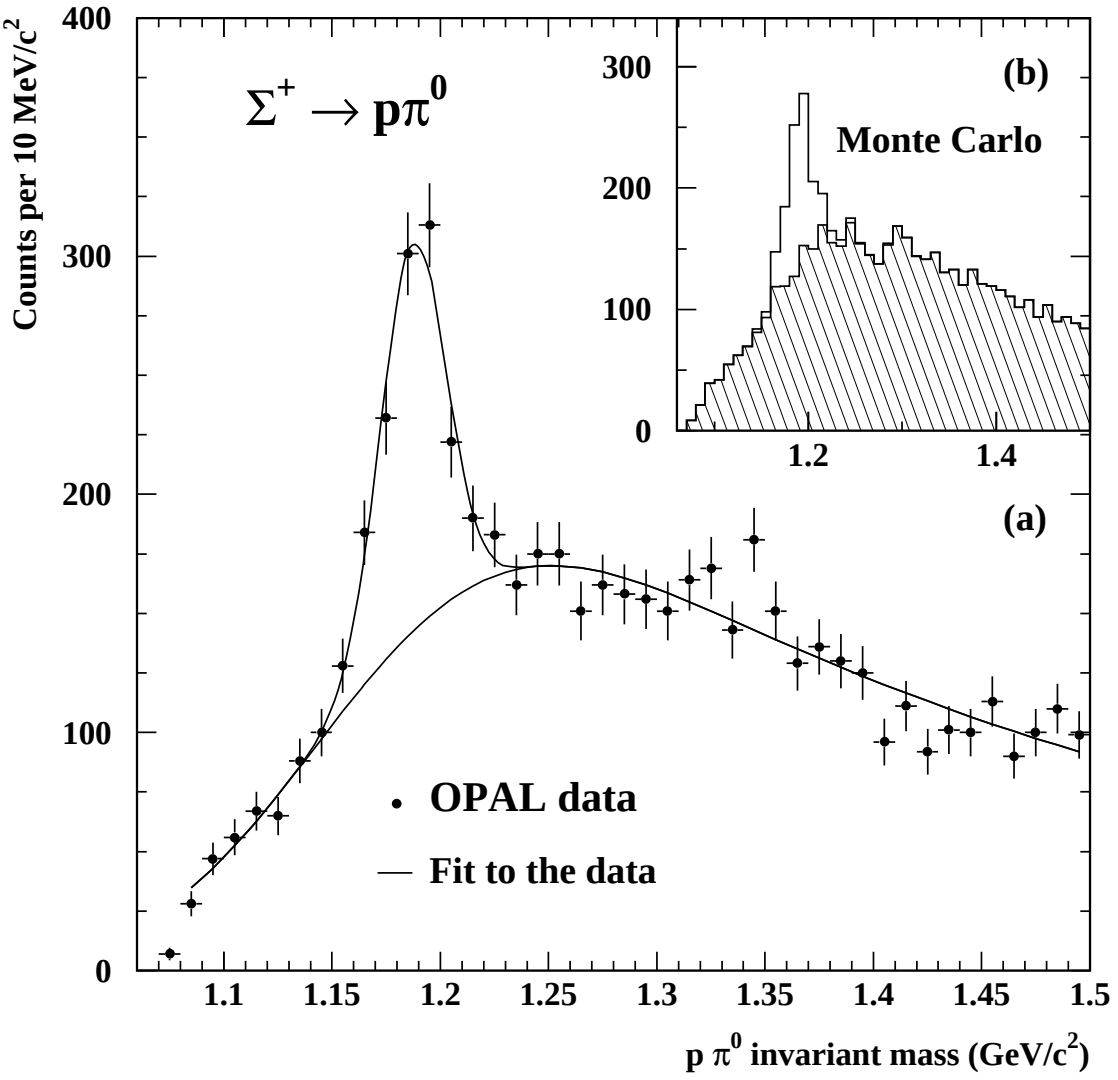

Figure 3: (a) Invariant mass distribution of proton and π^0 candidates, after the Σ^+ selection. The curves represent the fit to the data. (b) Invariant mass distribution of proton and π^0 candidates, after the Σ^+ selection, for the Monte Carlo sample (JETSET 7.3 and 7.4 with full detector simulation). The contribution from background events is shown hatched.

Table 2: Systematic errors on the integrated Σ^+ rate.

systematic error source	error contribution (%)
Monte Carlo statistics	4.5
BR($\Sigma^+ \to p\pi^0$)	0.6
Fit procedure	9.0
Cuts on proton track	2.6
Cuts in Σ^+ reconstruction	1.5
π^0 efficiency	5.0

were also repeated fixing the centroid of the signal Gaussian to 1189.4 MeV [14]. To reduce the effect of statistical fluctuations on the systematic errors deduced from these variations, the errors are evaluated for different values on the cuts on $\tilde{P}_{ij}$, and the average variation is taken as the systematic error. Errors associated with the fit procedure represent a 9.0% uncertainty on the integrated Σ^+ rate.

A systematic uncertainty is assigned to a possible discrepancy between data and Monte Carlo for quantities used in the selection. The number of protons and of Σ^+ candidates exclusively removed by a given cut are compared in the data and the Monte Carlo. For each cut, the discrepancy between the data and the Monte Carlo is scaled to the number of genuine Σ^+ removed, and this discrepancy is considered as a systematic error. The contributions of the track and Σ^+ cuts are 2.6 and 1.5 %, respectively. This error includes the effect of the uncertainty on the simulation of the z resolution of the vertex chamber and silicon microvertex detector. The systematic error on the π^0 efficiency is obtained by comparing the experimental $\tilde{P}_{ij}$ distributions for all π^0 candidates with the predictions of full simulations using JETSET 7.3 and HERWIG 5.5, as well as a version of JETSET 7.4 including $L = 1$ meson decays. Some discrepancies between the data and the different Monte Carlo samples are observed. They can partly be attributed to imperfections in the simulation of electromagnetic showers, but differences between the predicted density of tracks and electromagnetic clusters around the π^0 candidates play a role, as already recognised in refs. [15, 16]. These discrepancies amount to corrections that do not exceed 5% over the π^0 energy range relevant for this analysis ($0.5 < E_{\pi^0} < 5$ GeV), and this number is taken as the systematic error from this source. In addition, the cut on the variable $\tilde{P}_{ij}$ was varied from 0.050 to 0.200, and no significant variations in the rate were observed.

4.6 Integrated Rate

In the x_E range from 0.04 to 0.40, the integrated Σ^+ rate per hadronic Z^0 decay is:

$$n_{\Sigma^+}(0.04 < x_E < 0.40) \;=\; 0.078 \pm 0.006 \pm 0.010,$$

where the first error is statistical, and the second is systematic.

5 $\Sigma^0 \to \Lambda\gamma$ Analysis

The Σ^0 baryons are identified by their decay into $\Lambda\gamma$, where the $\Lambda \to p\pi^-$ decays are reconstructed as secondary vertices. In the decay $\Sigma^0 \to \Lambda\gamma$, the Λ carries away most of the Σ^0 momentum, leading to a relatively soft photon spectrum with an average energy of approximately 600 MeV. Therefore, conversions in the central tracking system are used, since they allow the low energy photons to be reconstructed with higher efficiency and better energy and spatial resolution than the electromagnetic calorimeter. Since the Σ^0 decays at the primary vertex, the Λ and γ momenta are constrained to point to that vertex.

5.1 Λ Selection

The Λ baryons are reconstructed from two oppositely charged tracks in the central tracking system, originating from a secondary vertex. The track selection and vertex reconstruction are identical to those used previously (method 2 in ref. [5]), except for the following changes which are designed to increase the efficiency and momentum resolution of the Λ sample:

- The impact parameter of the Λ relative to the primary vertex in the xy plane (d_0) is required to be less than 0.1 cm.
- The sum of the absolute values of the d_0 of the proton and pion tracks should be greater than 0.5 cm.
- The separation between the Λ decay vertex and the primary vertex in the xy plane should be between 1 and 150 cm.
- The angle in the xy plane between the Λ momentum and the vector from the primary vertex to the Λ decay point should be less than 5°.
- The pair is rejected if its invariant mass, assuming the tracks to be an electron and a positron, is smaller than 60 MeV/c^2. This cut serves to remove photon conversions from the Λ sample.
- The invariant mass of the Λ candidate is required to be within 10 MeV/c^2 of the nominal Λ mass [14], and its momentum must be between 0.75 and 20 GeV/c.

The resulting $p\pi^-$ mass spectrum is shown in figure 4a. After this selection, the resolution on the z component of the momentum vector of the Λ candidate is improved by constraining the Λ to originate from the primary vertex in z.

5.2 Photon Conversion Selection

The converted photons are reconstructed as two oppositely charged tracks in the central tracking system, originating from a secondary vertex. To increase the selection efficiency, the standard

track selection is relaxed to accept tracks with transverse momentum as low as 40 MeV/c and with as few as 20 hits in the jet chamber. The xy vertex of the photon conversion is defined as the midpoint between the tangents to the two tracks, at the points where they are parallel, in the xy plane. The separation between the two tracks at this point, Δ_{xy}, is required to be less than 5 cm. The difference in θ of the two tracks, Δ_θ, must be less than 1 radian. Finally, a hit is required on at least one of the tracks within 20 or 30 cm from the xy vertex, depending on whether this vertex is located in the vertex or jet chambers (corresponding to a radial distance from the primary vertex of < 27 cm and > 27 cm, respectively).

For surviving track pairs, a quantity, D, is calculated as:

$$D = \sqrt{(\frac{\Delta_{xy}}{xy_{90}})^2 + (\frac{\Delta_\theta}{\theta_{90}})^2} \qquad \text{if} \quad R_f < 27\,\text{cm, or}$$

$$D = \frac{\Delta_{xy}}{xy_{90}} \qquad \text{if} \quad R_f > 27\,\text{cm,}$$

where $\pm xy_{90}$ and $\pm\theta_{90}$ are the ranges of Δ_{xy} and Δ_θ, respectively, within which 90 % of the conversions are expected to occur, as determined by Monte Carlo simulation, and R_f is the smallest radius of any hit on either track. For each track, all possible combinations with other tracks satisfying all the previous cuts are studied, and the pair with the minimum value of D is selected.

A pair is selected as a photon candidate if it fulfils the following requirements:

- The value of D must be less than 2.
- The probability that the measured specific energy loss of each particle is consistent with the electron hypothesis is greater than 1.25 %.
- The secondary vertex must be separated from the primary vertex by more than 2 cm in xy to reject Dalitz pairs ($\pi^0 \to \gamma e^+ e^-$).
- The energy must be less than 1.5 GeV.

As for the Λ, the resolution on the mass of the photon candidate is improved by constraining the two tracks to originate from the same z coordinate, and the z-component of the momentum of the photon is improved by constraining the photon candidate to originate from the primary vertex in z. A photon candidate is accepted if its mass after that constraint is below 10 MeV/c^2. The mass spectrum of accepted photon candidates before the mass cut is shown in figure 4b.

5.3 Σ^0 Reconstruction

All Λ and γ candidates passing the above selection cuts are combined, and their invariant mass is determined. Combinations are accepted as Σ^0 candidates if the angle between the Λ and the γ is less than 1.5 radians in ϕ, and if they have no tracks in common. The invariant mass distribution of the accepted combinations is shown in figure 4c. The spectrum is fitted with a Gaussian to describe the signal and a third order polynomial times a threshold factor

$(m-(m_\Lambda+m_\pi))^{1/2}$ to describe the background. A signal of 220 $\pm$ 37 Σ^0 is observed at a mass of 1191 $\pm$ 1 MeV/c^2, which is consistent with the nominal value of 1192.6 MeV/c^2 [14]. The width of the peak (σ = 4.4 $\pm$ 0.9 MeV/c^2) is in agreement with that obtained in the Monte Carlo simulation (σ = 4.5 $\pm$ 0.2 MeV/c^2).

From the Monte Carlo sample, the selection efficiency is evaluated to be $(8.8 \pm 0.5)\times 10^{-4}$, yielding a total production rate of 0.071 $\pm$ 0.012 Σ^0 per hadronic Z^0 decay. Given the limited statistics, it is not possible to extract a significant differential cross-section from these data.

5.4 Consistency Checks and Systematic Errors

Several tests have been made to check the stability of the result. It was verified that the measured number of conversions per event is reproduced by the Monte Carlo at the level of 1.5 %. The Σ^0 rate is consistent for all years of data taking. In another test, photon candidates having a high probability to form a π^0 with another photon candidate detected in the electromagnetic calorimeter are removed from the sample. The Σ^0 rate obtained with this purer, but smaller, sample is entirely consistent.

The method for determining the number of Σ^0, the background parametrisation and the fit range were varied. Using the Monte Carlo sample, fits to the invariant mass distribution for all Σ^0 candidates or for only those that are truly Σ^0 were compared. The number of signal events was taken either as the fitted area of the Gaussian, or the area above the background within a $\pm 2\sigma$ mass window. All results are consistent, but from the observed deviations, a 9 % systematic uncertainty is assigned to the technique to evaluate the number of Σ^0 baryons.

The cuts on d_0 and invariant mass of the Λ candidates were varied, as well as those on the invariant mass and energy of the photon candidates. Although no significant systematic disagreement was found, from the observed deviations an 11 % systematic uncertainty is assigned to potential differences between the data and the Monte Carlo.

The average number of Σ^0 per hadronic Z^0 decay is thus:

$$n_{\Sigma^0} = 0.071 \pm 0.012 \pm 0.012,$$

where the first error is statistical, and the second is systematic and includes the Monte Carlo statistical uncertainty (0.004). According to the Monte Carlo simulation, this measurement is mostly sensitive to Σ^0 baryons in the x_E range from 0.05 to 0.4. An error on the uncertainty of the modelling of the x_E dependence of the cross-section by the Monte Carlo will be added: this will be discussed in section 7.

6 $\Sigma^- \to n\pi^-$ Analysis

Because the Σ^- and Σ^+ have relatively long lifetimes, a significant fraction of them decay inside the active volume of the jet chamber at a radius exceeding 25 cm. It is therefore possible to reconstruct charged Σ baryons in the decay $\Sigma^\pm \to n\pi^\pm$ by searching for the charged tracks of

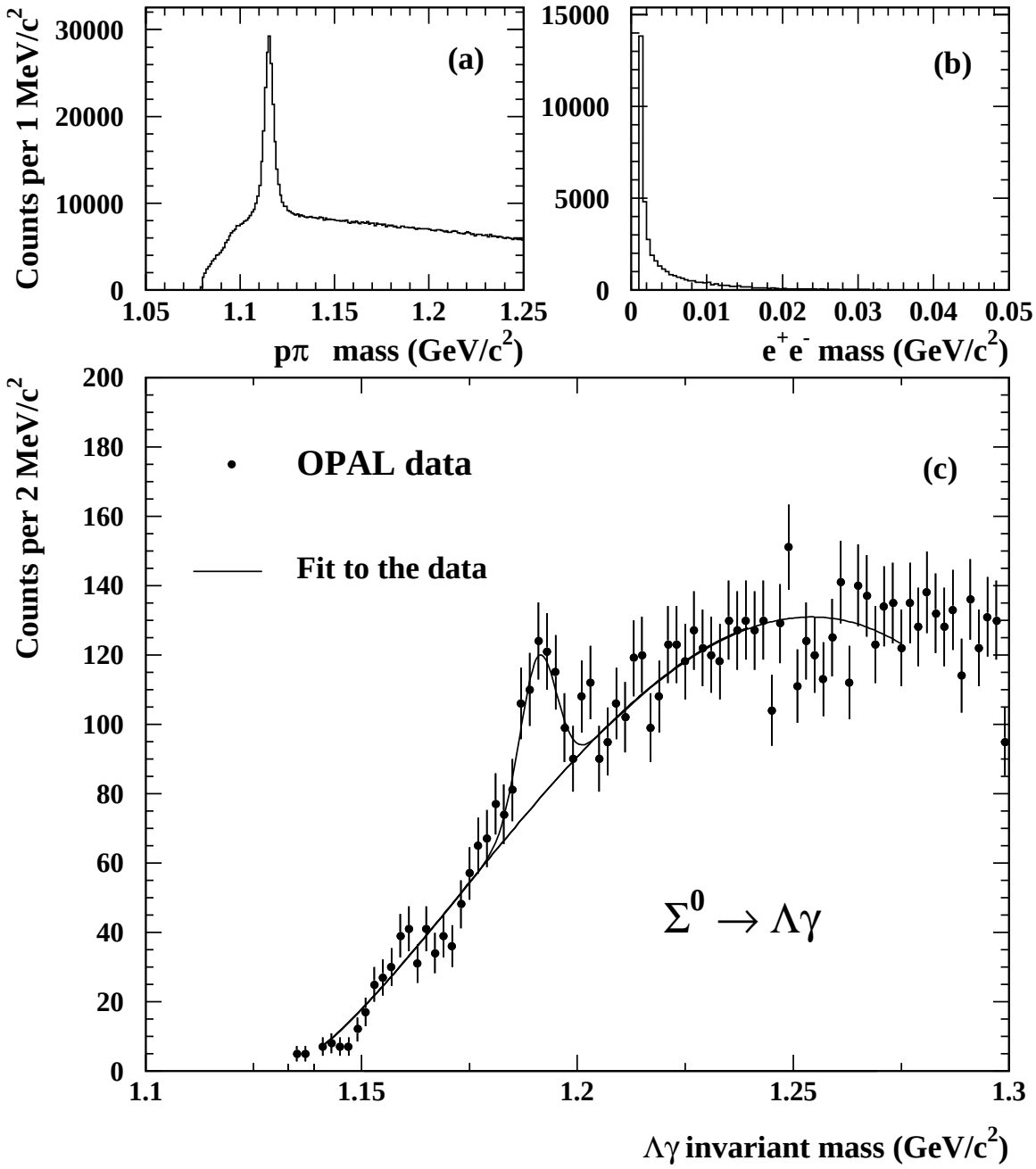

Figure 4: (a) Invariant mass distribution of $\Lambda \to p\pi^-$ candidates, before the Λ mass cut in the data. (b) Invariant mass distribution of e^+e^- pairs before the photon mass cut in the data. (c) Invariant mass distribution of $\Sigma^0 \to \Lambda\gamma$ candidates, after the Σ^0 selection. In (c) the points with error bars represent the OPAL data. The superimposed curves represent the result of the fit to the data (see text).

the Σ and its secondary π in this large volume chamber. If the decay angle, the angle between Σ and π at the decay vertex, is large enough, the parent and daughter charged particles are reconstructed as distinct tracks, which intersect inside the jet chamber. Since at least 10 jet chamber hits are needed for a track to be found, this method is sensitive only to Σ baryons decaying at a radius of at least 35 cm from the interaction point, therefore excluding low energy Σ baryons. Since the lifetime and $n\pi$ branching ratio of the Σ^- are both about twice that of the Σ^+, this method is clearly more sensitive to Σ^- decays. In fact, only 13 % of the selected sample are Σ^+ decays, and their contribution will be fixed to the rate as measured previously in section 4.

6.1 Secondary Vertex Reconstruction

The primary Σ and secondary π tracks are selected according to the following criteria:

- The xy components of the momenta of the primary and secondary tracks have to be larger than 150 MeV/c.
- Primary and secondary tracks have to fulfil the condition $|\cos\theta| < 0.75$.
- To reject unstable particles produced in hadronic interactions, it is required that the primary Σ track has a d_0 of less than 5 cm.

To find a candidate vertex, a search is made for the starting point of a secondary track within a 10 cm radius in xy around the end point of the primary track. If found, the intersection point of the track trajectories in the xy plane is taken as the position of the Σ decay vertex, where the distance to the primary vertex has to be greater than 35 cm. If there are two intersection points, the one closer to the endpoint of the primary track is used. Because the z resolution is not as good as the resolution in the xy plane, both tracks are constrained to a common z coordinate at the Σ decay vertex, and the primary track is additionally constrained to the z coordinate of the primary vertex.

In addition, the following requirements are made:

- To accommodate pattern recognition tolerances in cases where one track crosses the trajectory of another, the arc length of the part of the track beyond the intersection point (projected into the xy plane) should be less than 7 cm.
- Decay vertices with more than one secondary track are rejected, since they are likely to come from three-prong kaon decays or hadronic interactions with the material of the jet chamber.
- To reject the background caused by tracks re-entering the jet chamber from hadronic interactions in the conical endcaps of the chamber, the reconstructed decay vertex is required to be more than 34 cm away from these endcaps. This distance represents approximately 10 % of the jet chamber sense wire length.

- For all track pair candidates, a χ^2 is evaluated testing the agreement of the primary and secondary track parameters in the xy plane. Background candidates, especially those which are likely to be combinations of track pieces caused by the same charged particle but not merged by the pattern recognition, tend to have low χ^2 values and small decay angles. For that reason, candiates with a low χ^2 value or a decay angle less than 50 mrad are removed from the analysis.

- Finally, the sign of the charge of the Σ and π candidates must be the same.

After these cuts, the Monte Carlo predicts that almost all the secondary vertices are from either the decay in flight of a charged particle, or, to a lesser extent, from hadronic interactions in the jet chamber material. The combinatorial background due to the crossing of two unrelated tracks is very small and will be treated as a small correction to the hadronic background.

6.2 Neutron and $\Sigma^{\pm}$ Reconstruction

The momentum of the neutron candidate is calculated as the difference between the measured momenta of the Σ and the π tracks. Then, the energies of the pion and neutron candidates are obtained using their momenta and their known masses[14], and the invariant mass of the nπ system is evaluated.

6.3 Evaluation of the Background

The invariant mass alone is not sufficient to discriminate between genuine Σ^- decays and reflections due to the decays $\Xi^- \to \pi^-\Lambda$, $\pi^- \to \mu^-\overline{\nu}_\mu$, and the dominant kaon decays $K^- \to \mu^-\overline{\nu}_\mu$ and $K^- \to \pi^-\pi^0$. The production rate of the Ω^- is small enough[6] that it can be neglected. The lifetimes of the charged kaon and pion are orders of magnitude larger than that of the $\Sigma^{\pm}$ and, at momenta above 2 GeV/c, most of them decay outside the volume of the jet chamber. Monte Carlo simulations show that the background from π^- decays ($c\tau$ = 7.8 m) is negligible because the tracks cannot be resolved due to their small kink angle. However, the charged kaon ($c\tau$= 3.7 m) constitutes a major source of background.

The level of the kaon background in the sample is evaluated using two variables, in addition to the invariant mass (m) distribution. The first one is related to the proper time of the decay: it is the track length of the primary track divided by its momentum, s/p. The other is Θ^*, the decay angle of the pion candidate in the Σ rest frame, evaluated assuming a Σ hypothesis for the primary track. Fig. 5 shows how these three variables (m, s/p and Θ^*) can be used to evaluate the kaon background. The distribution of m and $\cos\Theta^*$ for a sample of Σ^- decays from the Monte Carlo simulation is shown in fig. 5a: most events are located in a vertical band centered at the mass of the Σ^-. The events coming from $K^{\pm} \to \mu^{\pm}\nu_\mu$ and $K^{\pm} \to \pi^{\pm}\pi^0$ decays have very different behaviour (fig. 5b): they are distributed along a curve, showing a strong correlation between m and Θ^*. The position of this curve is almost independent of the kaon momentum above 2 GeV/c. The existence of these two structures – the vertical band from $\Sigma^{\pm}$ decays and the curve from kaon decays – is clearly seen in the data (fig. 5c and 5d). To

better distinguish the kaon and $\Sigma^{\pm}$ populations, fig. 5c and 5d show events associated with short ($s/p < 15$ cm$\times c$/GeV) and long ($s/p > 15$ cm$\times c$/GeV) lifetimes, respectively. The kaon curve dominates the long lifetime plot, while a significant $\Sigma^{\pm}$ vertical band appears in the short lifetime plot. Another contribution associated with small s/p values are the decays of the Ξ^- into $\Lambda\pi^-$, forming an almost vertical band to the left of the Σ band, where they are strongly overlapping with kaons. Candidates from hadronic interactions with the jet chamber material populate the short as well as the long lifetime plot, where they are rather uniformly distributed with only a slight increase to negative $\cos\Theta^*$ values.

6.4 Evaluation of the Σ^- Rate.

To determine the Σ^- rate, the distributions in fig. 5c and 5d were each divided into 8 regions indicated by the straight lines. Out of these, 5 bins were composed as labelled in fig. 5c. The bins were chosen such that each had a different sensitivity to the relative yields from different sources, especially the Σ^-, as well as the background from kaon decays and from hadronic interactions. The Monte Carlo was used to predict the relative yield in these 2×5 bins for the following 6 different sources:

- the decay $\Sigma^- \to \mathrm{n}\pi^-$,
- the kaon decays $\mathrm{K}^- \to \mu^-\overline{\nu}_\mu$, $\mathrm{K}^- \to \pi^-\pi^0$, $\mathrm{K}^- \to e^-\overline{\nu}_e\pi^0$, $\mathrm{K}^- \to \mu^-\overline{\nu}_\mu\pi^0$ and $\mathrm{K}^- \to \pi^-\pi^0\pi^0$,
- the decay $\Xi^- \to \Lambda\pi^-$,
- the vertices from hadronic interaction within the detector material and the combinatorial background,
- the decay $\Sigma^+ \to \mathrm{n}\pi^+$,
- the secondary decays of charged particles (K^-, Σ^- and Ξ^-) which are produced in hadronic interactions.

The number of counts in the data bins was fitted using the sum of these 6 Monte Carlo distributions, where the first four were allowed a different normalisation in the maximum likelihood fit. The rate of the Σ^+, representing $\sim$13 % of all reconstructed Σ decays, was fixed to the value deduced from the $\mathrm{p}\pi^0$ measurement in section 4. In the x_E region above 0.4, where no Σ^+measurement via $\mathrm{p}\pi^0$ was possible, isospin symmetry for Σ^+ and Σ^- was assumed and a common normalisation for both particles determined by the fit. The very small contribution from secondary decays of charged particles generated in hadronic interactions of primary particles with the detector was fixed to the value predicted by the Monte Carlo.

It was possible to apply this procedure separately to 6 x_E bins ranging from 0.05 to 0.6. In each x_E bin, the cut on the parameter s/p was chosen to yield an optimum statistical discrimination between the Σ^- and the other sources. The quality of these 4-parameter fits can be judged from fig. 6, which shows the invariant mass distribution obtained by adding the

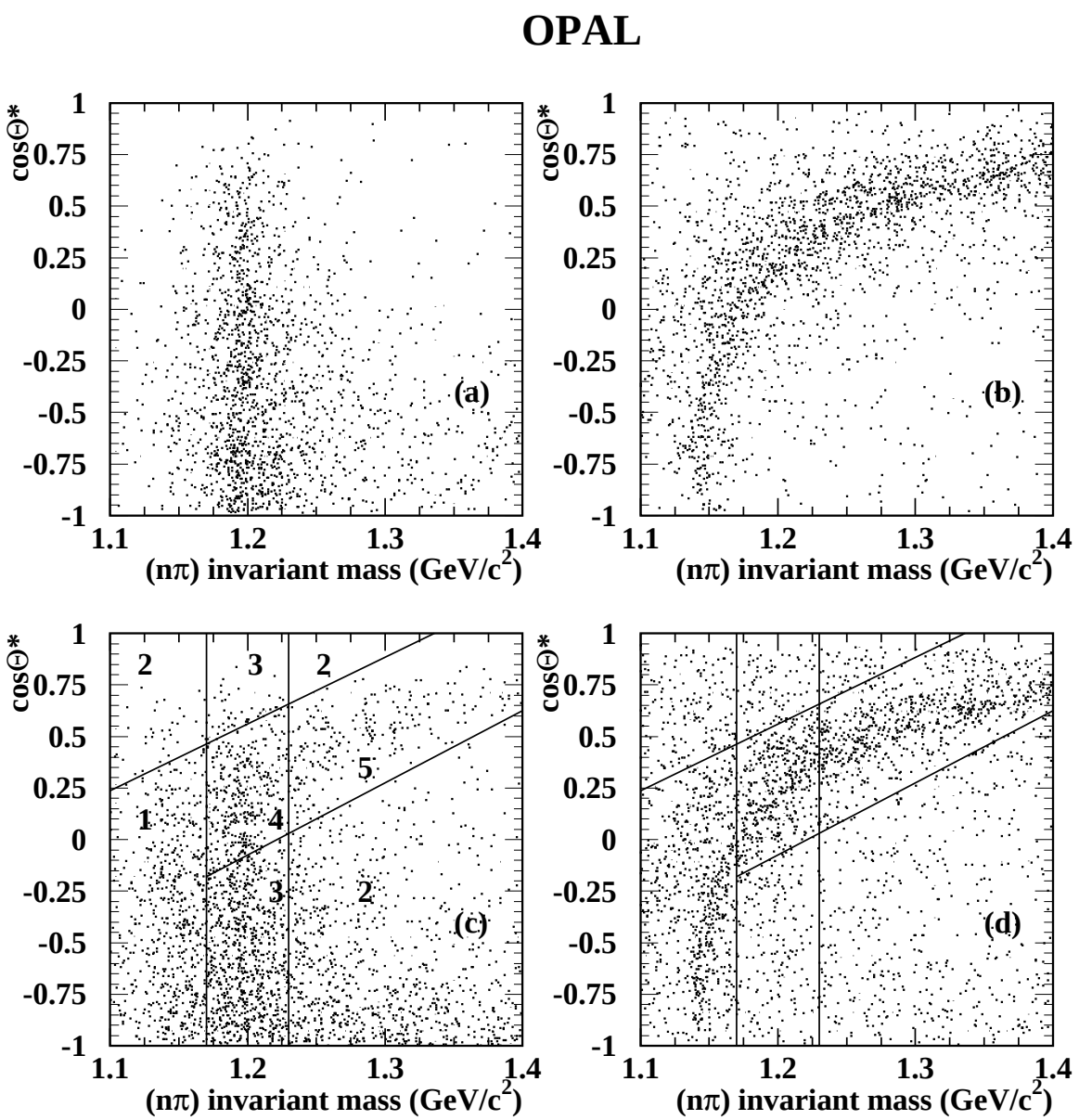

Figure 5: $\cos\Theta^*$ versus invariant mass, assuming the nπ hypothesis. (a) Monte Carlo simulation for $\Sigma \to$ nπ decays. (b) Monte Carlo simulation for $K^\pm \to \mu^\pm\nu_\mu$ and $K^\pm \to \pi^\pm\pi^0$ decays. (c) OPAL data for low s/p. (d) OPAL data (subsample) for high s/p. (In (c) and (d) the binning is shown as described in the text.)

Monte Carlo contributions according to the rates given by the fits for events in the low-lifetime bins. The sum of the contributions from the 6 x_E bins well represents the total data spectrum. The extracted x_E spectrum is shown in fig. 7.

6.5 Consistency Checks and Systematic Errors

An important systematic check is the comparison of the fitted Ξ^- and kaon rates with those already measured by more direct means. The small Ξ^- signal is very sensitive to systematic shifts in the kaon or $\Sigma^\pm$ shape. Nevertheless, the fitted rate, extrapolated over the entire x_E range (0.039 ± 0.013) is compatible with that of ref. [6] (0.0258 ± 0.0011). The inclusive $K^\pm$ rate obtained in our fit (2.37 ± 0.58) agrees with that of ref. [17] (2.42 ± 0.13), and so does the differential cross-section. Since it is also possible to measure the kaon differential cross-section for x_E values below 0.05, as an additional check the same analysis optimised for kaon identification was applied in the x_E range from 0.012 to 0.300. The inclusive $K^\pm$ rate (2.24 ± 0.20) and the differential cross-section obtained from that are found to be in a good agreement with the corresponding results of the Σ^- analysis presented here, and with that of ref. [17] given above.

The systematic errors for the Σ^- analysis are evaluated in the same way as for the Σ^+ measurement in section 4, taking the average variation observed while changing the relevant quantity. They are listed in table 3.

One might expect a sensitivity of the results on the fiducial volume, because an increasing rate has to be folded with a decreasing efficiency near the inner radius. However, the result was found to be stable against variations of acceptance cuts for the position of the secondary vertex, which have been varied along the z axis and the inner radius by 8 and 10 cm, respectively.

There are cases in which the pattern recognition is unable to resolve the two tracks and combines them into one. The critical parameter for this effect is the decay angle. The corresponding distribution for values above 50 mrad is found to be well described by the Monte Carlo simulation, so the resulting systematic error is relatively small. In addition, some dependence of the result on the gap size between the two tracks is observed, which indicates that the modelling of tracks and their reconstruction is not perfect if the secondary track is steeply inclined with respect to the wire planes of the drift chamber.

The wide mass distribution introduces a correlation between the deduced Σ^- rate and the mass resolution, dominated by the uncertainty in θ, the measured polar angles of the tracks. The resolution of θ was determined in a fit to the data, and the change in the Σ^- rate observed while varying the resolution of θ within one standard deviation was taken as the systematic error for this source.

To derive the uncertainty arising from the Σ^+ production rate and the Σ^- lifetime used in this analysis, these quantities were varied within their errors, and the observed variation of the result taken as the systematic error.

The efficiency-corrected rates of Σ^- per hadronic Z^0 decay are shown in bins of x_E in table 4.

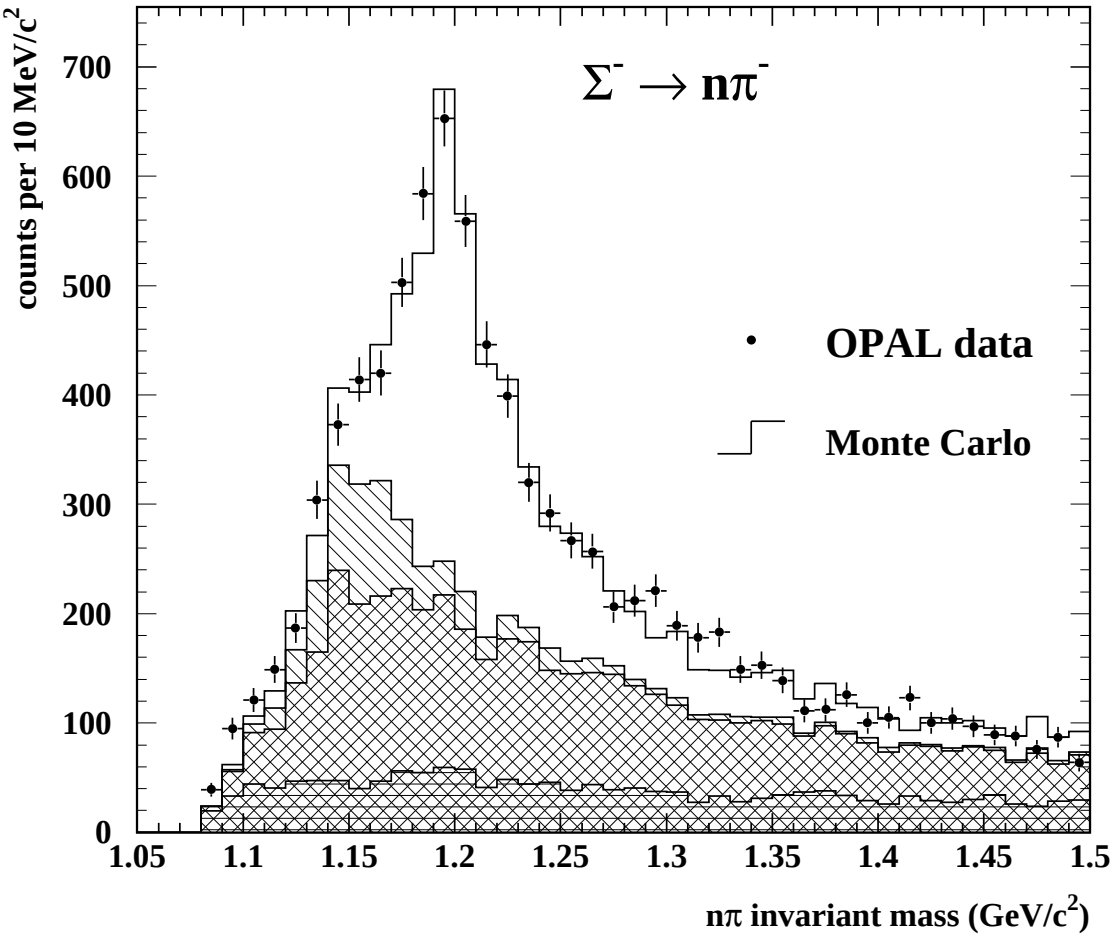

Figure 6: Invariant nπ mass distribution for the selected track pairs in the x_E range from 0.05 to 0.6. The solid line shows the prediction by the Monte Carlo, obtained by summing the contributions from the six sources discussed in the text and normalised using the result of the fit to the data in each of the 6 x_E bins. The white area under the histogram represents the contributions from Σ^+ and Σ^-; the hatched area: the contribution from Ξ^-; the doubly-hatched area: the kaon contribution. The triply-hatched area represents the background from hadronic interactions, from secondary decays of charged particles generated in hadronic interactions and the combinatorial background.

Table 3: Systematic errors on the integrated Σ^- rate.

systematic error source	error contribution (%)
minimum radius of decay vertex	1.5
vertex distribution along z	0.5
decay angle acceptance	1.0
gap between tracks	2.0
resolution on θ	7.0
constrained Σ^+ rate	3.5
uncertainty in Σ lifetime	2.0
simulation of other cuts	4.0

x_E bin	Number of Σ^- in data	Efficiency (%)	Differential Cross-Section $\frac{1}{\sigma_{had}}\frac{d\sigma}{dx_E}$ ($\pm$ stat. $\pm$ syst. errors)
0.050 - 0.100	585 $\pm$ 109	0.701 $\pm$ 0.067	0.480 $\pm$ 0.073 $\pm$ 0.052
0.100 - 0.150	806 $\pm$ 110	2.02 $\pm$ 0.15	0.229 $\pm$ 0.028 $\pm$ 0.015
0.150 - 0.200	762 $\pm$ 95	3.02 $\pm$ 0.23	0.145 $\pm$ 0.013 $\pm$ 0.012
0.200 - 0.300	954 $\pm$ 136	3.52 $\pm$ 0.27	0.0780 $\pm$ 0.0070 $\pm$ 0.0087
0.300 - 0.400	436 $\pm$ 116	3.03 $\pm$ 0.35	0.0414 $\pm$ 0.0064 $\pm$ 0.0089
0.400 - 0.600	238 $\pm$ 65	1.77 $\pm$ 0.30	0.0193 $\pm$ 0.0025 $\pm$ 0.0047

Table 4: Number of Σ^- (determined by the fit), Σ^- detection efficiency (in per cent) and differential cross-section $\frac{1}{\sigma_{had}}\frac{d\sigma}{dx_E}$ in bins of x_E.

6.6 Integrated Rate

In the x_E range from 0.05 to 0.6, the integrated Σ^- rate per hadronic Z^0 decay is:

$$n_{\Sigma^-}(0.05 < x_E < 0.60) = 0.058 \pm 0.004 \pm 0.006,$$

where the errors are statistical and systematic, respectively.

7 Σ^+, Σ^0 and Σ^- Inclusive Rates and Differential Cross-Sections

The measured differential cross-sections for Σ^+ and Σ^- are shown in fig. 7 together with the predictions of the JETSET 7.4 [1] and HERWIG 5.5 [2] Monte Carlo programs with default input parameters, normalised to the measured rate of the relevant baryon[3]. Within errors, the shape of the x_E distributions is well described by JETSET and HERWIG.

The data for the two isospin states agree within errors. Since the Σ^+ and Σ^- data overlap in the region $0.05 < x_E < 0.40$, for the first time it is possible to compare directly the Σ^+ and Σ^- production rates in e^+e^- annihilation. The ratio of the Σ^+ to the Σ^- cross-section in this x_E range is 1.26 ± 0.14 (stat.) $\pm$ 0.16 (syst.). This ratio is compatible with the predictions of JETSET 7.4 and HERWIG 5.5 (1.08 and 1.24, respectively), but does not exclude a ratio of 1 which would correspond to the case of full isospin symmetry.

Extending the measurements to cover the entire x_E range requires some assumptions regarding the extrapolation to high and low values of x_E. In the default version of JETSET, 3.8 % (0.7 %) of the Σ^+ and Σ^- are produced at x_E values larger than 0.4 (0.6), and 18.1 % (28.3 %) with an x_E smaller than 0.04 (0.05), respectively. We use these fractions to correct the measured rates. If HERWIG is used instead for the extrapolation, very similar rates are obtained. As a systematic uncertainty we take the difference between the rates obtained by this procedure and an extrapolation performed using the shape of the Λ differential cross-section as measured by OPAL [6]. The individual rates evaluated over the entire x_E range for the Σ^+ and Σ^- are thus determined to be:

$$\begin{aligned} n_{\Sigma^+} &= 0.099 \pm 0.008 \pm 0.012 \pm 0.004 \qquad (0 < x_E < 1) \\ n_{\Sigma^-} &= 0.083 \pm 0.006 \pm 0.008 \pm 0.004 \qquad (0 < x_E < 1), \end{aligned}$$

where the first error is statistical, the second systematic and the third is from the extrapolation. These results are compared with predictions of different models in table 5. Although somewhat larger, the measured rates are nevertheless compatible within 2 standard deviations with the corresponding rates in JETSET 7.4, HERWIG 5.5 and the thermodynamical model of ref. [18] (see table 5).

[3]The prediction of the JETSET versions 7.4 and 7.3 differ by < 4 % in the inclusive rate, and by < 1 % in the relative shape of the x_E distribution.

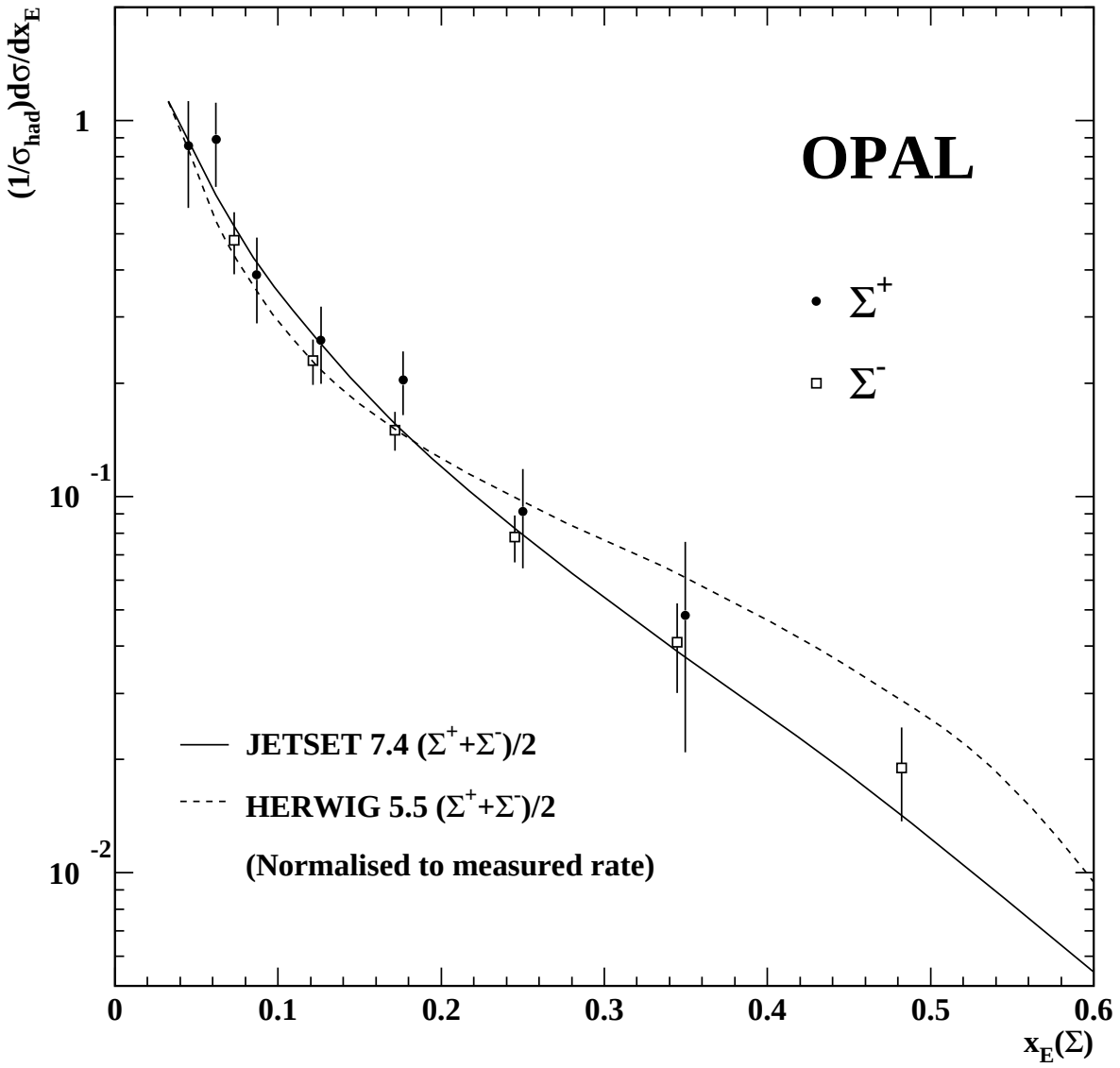

Figure 7: Fractional energy spectrum for Σ baryons. The plotted error bars represent the quadratic sum of the statistical and systematic errors. The curves show different Monte Carlo predictions, normalised to the average number of observed Σ^+ and Σ^-. The Monte Carlo curves have been calculated using the same binning as in the data. Solid line: JETSET 7.4; dashed line HERWIG 5.5.

Given that the shape of the x_E distribution is well reproduced by JETSET for both Σ^+ and Σ^-, we assume that this is also the case for the Σ^0 over the x_E range covered by all three measurements ($0.05 < x_E < 0.4$). Including an equivalent extrapolation error to cover the regions at low and high x_E where the efficiency for Σ^0 reconstruction is very low, the resulting inclusive rate for Σ^0 is:

$$n_{\Sigma^0} \;=\; 0.071 \pm 0.012 \pm 0.012 \pm 0.004 \qquad (0 < x_E < 1).$$

This is again compatible with the JETSET and HERWIG predictions of 0.073 and 0.056, respectively.

If full isospin symmetry is assumed in the production of the charged states, the extrapolation error is minimised owing to the different x_E bins covered by the analyses, and the averaged inclusive rate is:

$$\overline{n}_{\Sigma^\pm} = \frac{1}{2}[n_{\Sigma^+ + \Sigma^-}] = 0.087 \pm 0.005 \text{ (stat.)} \;\pm 0.007 \text{ (syst.)} \;\pm 0.003 \text{ (extrap.)}.$$

Adding to this the result for Σ^0, we obtain:

$$\overline{n}_{\Sigma} = \frac{1}{3}[n_{\Sigma^+ + \Sigma^0 + \Sigma^-}] = 0.084 \pm 0.005 \text{ (stat.)} \;\pm 0.007 \text{ (syst.)} \;\pm 0.003 \text{ (extrap.)}.$$

The same result is obtained if isospin symmetry is not assumed and a straight average of the three rates is performed. The present results are consistent with the overall $\Sigma^\pm$ and Σ^0 rates quoted in ref. [7] by the DELPHI Collaboration.

particle	DELPHI	OPAL	JETSET 7.4	HERWIG 5.6	Therm. Model
Σ^+	-	0.099 ± 0.015	0.072	0.072	0.077
Σ^0	0.070 ± 0.014	0.071 ± 0.018	0.073	0.056	0.077
Σ^-	-	0.083 ± 0.011	0.067	0.060	0.069
$\frac{1}{2}[\Sigma^+ + \Sigma^-]$	0.085 ± 0.031	0.087 ± 0.009	-	-	-
$\frac{1}{3}[\Sigma^+ + \Sigma^0 + \Sigma^-]$	0.073 ± 0.013	0.084 ± 0.009	-	-	-

Table 5: Inclusive Σ yields in the data compared with published results of other LEP experiments [7], with Monte Carlo models and the thermodynamical model of ref. [18]. For the evaluation of the combined rates, isospin symmetry is assumed.

In ref. [6], the rates of other strange baryons are compared to the prediction of the JETSET di-quark model as implemented in JETSET. It was found that the model could not simultaneously describe the production rates of all $J^P = \frac{3}{2}^+$ baryons. With the present measurement of the Σ production rate, it is possible to study the extra suppression of strangeness in di-quarks in both the $J^P = \frac{1}{2}^+$ decuplet and $J^P = \frac{3}{2}^+$ octet. We consider the following double ratio, which should be close to 1 if the suppression of all strange quarks is the same in $J^P = \frac{1}{2}^+$ and $J^P = \frac{3}{2}^+$ Σ and Ξ baryons:

$$r = \frac{(\overline{n}_{\Xi} - BR(\Xi^*(1530) \to \Xi) \times \overline{n}_{\Xi^*(1530)})}{(\overline{n}_{\Sigma} - BR(\Sigma^*(1385) \to \Sigma) \times \overline{n}_{\Sigma^*(1385)})} \times \frac{\overline{n}_{\Sigma^*(1385)}}{\overline{n}_{\Xi^*(1530)}}. \qquad (2)$$

The ratio r is calculated taking into account corrections to the rates of the Ξ and Σ due to the feed-down from the corresponding $J = \frac{3}{2}$ state ($BR(\Sigma^*(1385) \to \Sigma) = 0.12$, and $BR(\Xi^*(1530) \to \Xi) = 1$ [14]). According to JETSET, the effect of other feed-down decays is small.

Our measurement, combined with the recent OPAL measurements of other strange baryon rates [6], yields an r value of 0.83 ± 0.13. This number is consistent with the ratios computed from the measurements at a centre-of-mass energy of 10 GeV [4] ($r = 0.92 \pm 0.48$ on the Υ, and 0.86 ± 0.51 on the continuum), and from the results of the DELPHI collaboration [7] (1.38 ± 0.41), with a substantially smaller error.

Our measured ratio is substantially smaller than the prediction of 2.5 from JETSET 7.4. That prediction is not affected appreciably by variation of the parameters controlling *i)* the di-quark creation probability, *ii)* the overall supression of strangeness, *iii)* the suppression of spin-1 diquarks, or *iv)* the popcorn mechanism [4]. However, it is almost inversely proportional to the value of the parameter controlling *v)* the extra suppression of strange quarks within di-quarks [5]. Within the simplest implementation of the di-quark model in JETSET, the measured ratio is incompatible with any sizeable extra suppression of strange quarks within di-quarks. In HERWIG, there is no extra suppression mechanism for s quarks in baryons, and it predicts a ratio of 1.1. However, HERWIG cannot reproduce the observed rates of the individual baryons, while JETSET with a proper tune of parameters *i)* to *v)* can reproduce at least three of the four rates. The failure of JETSET to reproduce the combined ratio of the Σ, Ξ, $\Sigma^*(1385)$ and $\Xi^*(1530)$ may indicate that the extra suppression of strangeness in di-quarks is not the most effective way to reproduce the production rates of strange baryons.

8 Summary

The production rates of the $J^P = \frac{1}{2}^+$ octet Σ baryons in hadronic Z^0 decays have been measured using the OPAL detector at LEP. The inclusive production rates of the three isospin states have been separately measured for the first time, and are

$$\begin{aligned} n_{\Sigma^+} &= 0.099 \pm 0.008 \pm 0.013 \\ n_{\Sigma^0} &= 0.071 \pm 0.012 \pm 0.013 \\ n_{\Sigma^-} &= 0.083 \pm 0.006 \pm 0.009, \end{aligned}$$

where the first error is statistical, and the second systematic, including the uncertainty in the extrapolation for the unobserved baryon energy range. These rates are consistent with the expectations of both the JETSET 7.4 and HERWIG 5.5 event generators. Within errors, the shape of the x_E distributions is well described by JETSET and HERWIG. If full isospin symmetry is assumed in the production of the 3 states, the extrapolation error is minimised due to the different x_E bins covered by the analysis, and the average inclusive rate is:

$$\overline{n}_\Sigma = \frac{1}{3}[n_{\Sigma^+ + \Sigma^0 + \Sigma^-}] = 0.084 \pm 0.005 \text{ (stat.)} \ \pm 0.008 \text{ (syst.)} \ .$$

[4] Respectively, the parameters PARJ(1), PARJ(2), PARJ(4) and PARJ(5) in JETSET.

[5] The parameter PARJ(3) in JETSET, whose default value is 0.4.

This rate, combined with the recent measurements of the Σ^*, Ξ and Ξ^* baryons [6], is incompatible with the sizeable extra suppression of strangeness in diquarks that is present in the default versions of the di-quark model of JETSET [1].

Acknowledgements

We particularly wish to thank P. Eden and T. Sjöstrand for helpful discussions concerning the JETSET di-quark model. It is a pleasure to thank the SL Division for the efficient operation of the LEP accelerator and for their continuing close cooperation with our experimental group. In addition to the support staff at our own institutions we are pleased to acknowledge the
Department of Energy, USA,
National Science Foundation, USA,
Particle Physics and Astronomy Research Council, UK,
Natural Sciences and Engineering Research Council, Canada,
Israel Ministry of Science,
Israel Science Foundation, administered by the Israel Academy of Science and Humanities,
Minerva Gesellschaft,
Japanese Ministry of Education, Science and Culture (the Monbusho) and a grant under the Monbusho International Science Research Program,
German Israeli Bi-national Science Foundation (GIF),
Direction des Sciences de la Matière du Commissariat à l'Energie Atomique, France,
Bundesministerium für Bildung, Wissenschaft, Forschung und Technologie, Germany,
National Research Council of Canada,
Hungarian Foundation for Scientific Research, OTKA T-016660, and OTKA F-015089.

References

[1] B. Andersson *et al.*, Phys. Rep. **97** (1983) 31;
T. Sjöstrand, Comp. Phys. Comm. **39** (1986) 347;
T. Sjöstrand and M. Bengtsson, Comp. Phys. Comm. **43** (1987) 367;
T. Sjöstrand, Comp. Phys. Comm. **82** (1994) 74.

[2] G. Marchesini and B.R. Webber, Nucl. Phys. **B310** (1988) 461;
G. Marchesini, B.R. Webber *et al.*, Comp. Phys. Comm. **67** (1992) 465.

[3] S. B. Chun and C.D. Buchanan, Phys. Lett. **B308** (1993) 153.

[4] ARGUS Collaboration, H. Albrecht et al., Phys.Lett. **183B** (1987) 419;
ARGUS Collaboration, H. Albrecht et al., Z. Phys. **C9** (1988) 177.

[5] OPAL Collaboration, P.D. Acton *et al.*, Phys. Lett. **B305** (1993) 415;

[6] OPAL Collaboration, G. Alexander *et al.*, CERN-PPE/96-99.

[7] DELPHI Collaboration, P. Abreu *et al.*, Z. Phys. **C67** (1995) 543;
DELPHI Collaboration, W. Adam *et al.*, Z. Phys. **C70** (1996) 371.

[8] OPAL Collaboration, K. Ahmet *et al.*, Nucl. Instr. and Meth. **A305** (1991) 275.

[9] P.P. Allport *et al.*, Nucl. Instr. and Meth. **A324** (1993) 34;
P.P. Allport *et al.*, Nucl. Instr. and Meth. **A346** (1994) 476.

[10] M. Hauschild *et al.*, Nucl. Instr. and Meth. **A314** (1992) 74.

[11] OPAL Collaboration, G. Alexander *et al.*, Z. Phys. **C52** (1991) 175.

[12] OPAL Collaboration, G. Alexander *et al.*, Z. Phys. **C69** (1996) 543;
OPAL Collaboration, P.D. Acton *et al.*, Z. Phys. **C58** (1993) 387;
OPAL Collaboration, M.Z. Akrawy *et al.*, Z. Phys. **C47** (1990) 505.

[13] J. Allison *et al.*, Nucl. Instr. and Meth. **A317** (1992) 47.

[14] The Particle Data Goup, L. Montanet *et al.*, Phys. Rev. **D50** (1994) 1173.

[15] L3 Collaboration, A. Adam *et al.*, Phys. Lett. **B328** (1994) 223.

[16] DELPHI Collaboration, W. Adam *et al.*, Z. Phys. **C69** (1996) 561.

[17] OPAL Collaboration, R. Akers *et al.*, Z. Phys. **C63** (1994) 181.

[18] F. Becattini, Z. Phys. **C69** (1996) 485.
The quoted results were obtained directly from the author.